AGU PUBLICATIONS

Geophysical Research Letters

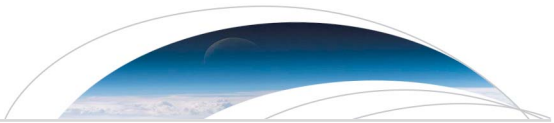

RESEARCH LETTER
10.1002/2017GL076056

Key Points:
- Sea ice deformation is a major driver of the sea ice volume gain in winter
- The winter storm studied here contributed to 0.5% increase of sea ice volume and 1.3% increase in deformed sea ice fraction

Supporting Information:
- Supporting Information S1

Correspondence to:
P. Itkin,
polona.itkin@npolar.no

Citation:
Itkin, P., Spreen, G., Hvidegaard, S. M., Skourup, H., Wilkinson, J., Gerland, S., & Granskog, M. A. (2018). Contribution of deformation to sea ice mass balance: A case study from an N-ICE2015 storm. *Geophysical Research Letters*, *45*, 789–796. https://doi.org/10.1002/2017GL076056

Received 29 OCT 2017
Accepted 12 DEC 2017
Accepted article online 28 DEC 2017
Published online 17 JAN 2018

Contribution of Deformation to Sea Ice Mass Balance: A Case Study From an N-ICE2015 Storm

Polona Itkin[1], Gunnar Spreen[1,2], Sine Munk Hvidegaard[3], Henriette Skourup[3], Jeremy Wilkinson[4], Sebastian Gerland[1], and Mats A. Granskog[1]

[1]Norwegian Polar Institute, Fram Centre, Tromsø, Norway, [2]Institute of Environmental Physics, University of Bremen, Bremen, Germany, [3]National Space Institute (DTU Space), Technical University of Denmark, Kgs. Lyngby, Denmark, [4]British Antarctic Survey, Cambridge, UK

Abstract The fastest and most efficient process of gaining sea ice volume is through the mechanical redistribution of mass as a consequence of deformation events. During the ice growth season divergent motion produces leads where new ice grows thermodynamically, while convergent motion fractures the ice and either piles the resultant ice blocks into ridges or rafts one floe under the other. Here we present an exceptionally detailed airborne data set from a 9 km^2 area of first year and second year ice in the Transpolar Drift north of Svalbard that allowed us to estimate the redistribution of mass from an observed deformation event. To achieve this level of detail we analyzed changes in sea ice freeboard acquired from two airborne laser scanner surveys just before and right after a deformation event brought on by a passing low-pressure system. A linear regression model based on divergence during this storm can explain 64% of freeboard variability. Over the survey region we estimated that about 1.3% of level sea ice volume was pressed together into deformed ice and the new ice formed in leads in a week after the deformation event would increase the sea ice volume by 0.5%. As the region is impacted by about 15 storms each winter, a simple linear extrapolation would result in about 7% volume increase and 20% deformed ice fraction at the end of the season.

1. Introduction

Sea ice dynamics is highly coupled to the internal stress of the ice pack for a given region, which in turn is modified by inherent properties of sea ice such as strength, thickness, and floe size distribution (Thorndike, 1986). In compact pack ice sea ice drift can cause deformation events that influence the distribution of ice thickness through the generation of areas of open water (e.g., leads) in divergent regimes, and sea ice rafting and ridging in shear and convergent regimes. It has been suggested that majority of new ice formed during the winter originates from the refreezing of leads (Maykut, 1986), while the redistribution of ice piled into pressure ridges to accommodate the leads can constitute 30% of sea ice exported through the Fram Strait (Hansen et al., 2013).

However, Arctic sea ice is changing, it is getting thinner (Kwok & Cunningham, 2015), more dynamic (Spreen et al., 2011), and at the same time the deformation processes are increasing (Itkin et al., 2017; Rampal et al., 2009). These changes should lead to an increase in the contribution of deformed sea ice in the distribution of first year sea ice thickness. Still, the difficulties in performing routine ice thickness observations over large spatial scales mean that the separating thermodynamic and dynamic processes are difficult. Such studies would be of a high value for the climate modeling community, where processes can be studied individually. A notable exception is the recent large-scale study of Kwok and Cunningham (2016), who used monthly averages of the satellite remote sensing data for the sea ice thickness and drift for the region north of Canadian Arctic Archipelago and Greenland and estimated that the combination of pressure ridging and new ice formation explained about half the total sea ice thickness change for five winters between 2011 and 2015.

Sea ice usually deforms and redistributes during temporally discrete atmospheric driven events like storms and abrupt wind direction changes (Hutchings et al., 2011; Itkin et al., 2017). Here we present a detailed local-scale study of a single deformation event that enabled us to determine a relationship between the deformation and the redistribution of sea ice mass. If this relationship is representative for other regions, it can be used for upscaling other deformation events under similar conditions.

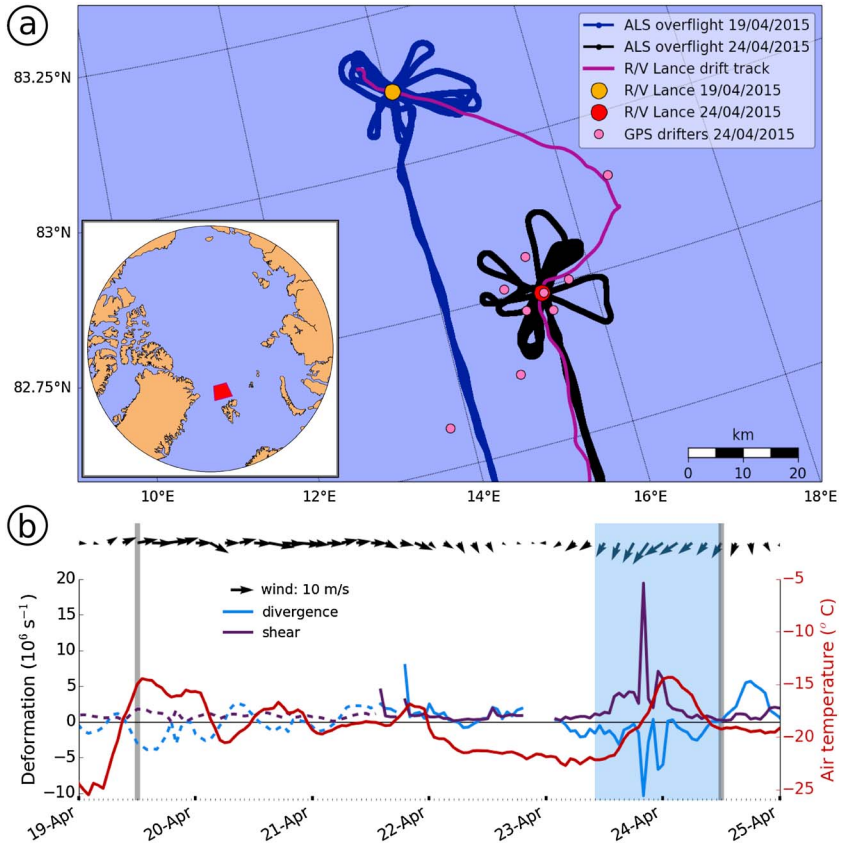

Figure 1. Overview of (a) region of interest with flight lines, R/V *Lance* drift, and GPS drifter array positions during the second overflight and (b) time series of meteorological observations and deformation rates. The wind data are from the meteorological mast on R/V *Lance* (Hudson et al., 2015), and the duration of storm event (Cohen et al., 2017) is shaded in blue. Dashed lines at the beginning of time series depict divergence and shear at the largest scale (~100 km) of the GPS drifter array. From 21 April deformation is shown at the smaller scale (15–10 km) by solid lines. The overflight timings are marked by gray vertical lines.

2. Data and Methods

This work is based on the laser scanner data collected on Ice, Climate, Economics-Arctic Research on Change (ICE-ARC) flights on 19 and 24 April 2015 (hereafter, first and second overflight represented by flight lines in Figure 1a). These flights centered on the R/V *Lance* that was frozen in the ice as part of the Norwegian young sea ICE (N-ICE2015) expedition (Granskog et al., 2016). In order to obtain complete coverage of three-dimensional surface topography over a ~9 km^2 survey region of sea ice around the R/V *Lance*, a series of overlapping flight lines were performed. Importantly, the first overflight occurred before the storm-driven deformation event, while the second overflight occurred just after the deformation event (Figure 1b).

Surface topographic height measurements were obtained using an airborne Laser Scanner (ALS, Riegl LMS Q240i-80) that was installed on the British Antarctic Survey's Twin Otter airplane. At 300 m flight altitude this resulted in ~1 m resolution and swath width of 450 m. From these distance measurements we derived surface elevations using GPS positioning and inertial navigation attitude information. The resulting point cloud of elevations was then referred to the local sea surface first by subtracting a local geoid model (from the Arctic Gravity Project) and then identifying minimum elevation in the data corresponding to open water or thin refrozen leads (Hvidegaard & Forsberg, 2002). Finally, we fitted a smooth function to the selected minimum values and subtracted it from the elevations. This resulted in snow freeboards (elevations of the air/snow surface above the ocean surface)—hereafter, freeboards. The precision of the data (data compared to data obtained during the same flight) is 0.01 m, while the accuracy (comparing data from different flights) is in the range of 0.1–0.2 m. To improve the accuracy and to be able to detect relatively small changes of freeboards between the overflights, we applied postprocessing corrections, details of which are described in the supporting information.

The airplane overflew R/V *Lance* and the surrounding sea ice covered area in "mowing-the-lawn" pattern so that the adjacent swaths could be connected into a three-dimensional mosaic over the survey region. To correct for sea ice drift during consecutive flight lines, we used the GPS position and time data from the airplane and the ship. The data were then interpolated to a 5 m × 5 m grid by nearest neighbor interpolation. The resultant freeboard maps for each overflight can be seen in Figures 2a and 2b.

To set up a reference frame, we manually identified 113 virtual buoys by visual matching of prominent features in the surface topography that were preserved between both overflights. These features were mainly ridge sails, and they were selected in a way that any three virtual buoys form a triangle with side length roughly between 100 and 500 m (Figures 2a and 2b). We then performed a Delauney triangulation between the virtual buoys of the first overflight and conserved the same triangulation for the second overflight. By such means we matched a total survey region area of 9.05 km^2 and an irregular grid of 158 triangles with mean area A = 58,000 m^2.

To avoid introducing further uncertainties by estimating sea ice thickness from freeboard, we decided to use the freeboard change between the overflights as a measure of ice mass redistribution. To be able to do that we assumed that snow depth, snow density, and ice density did not change significantly in the 5 day window between the overflights. The temperatures before and after the storm were below −20°C. There was no snowfall during the storm (Cohen et al., 2017), and in situ measurements confirmed that snow redistribution caused by strong winds had no significant influence on the mean snow depth (Rösel et al., 2016) and thus can be neglected.

We also argue that all the detected changes in freeboard between the overflights were due to mechanical redistribution of sea ice mass from the deformation event. We estimated the thermodynamical sea ice growth based on an empirical formula of Lebedev (Maykut, 1986). There sea ice thermodynamical growth $\Delta h_t = 1.33\Theta^{0.58}$ (cm) is determined from the freezing degree days $\Theta = \int (T_s - T_0)dt$, where $T_s = -20°C$ is surface air temperature and $T_0 = -1.9°C$ is freezing temperature of sea water. This yields in a maximum of 0.18 m of sea ice formed in 5 days in the newly opened leads. In refrozen leads and in older snow-covered ice the growth would be lower. For ice not covered by snow this will yield in 0.02 m freeboard change Δh_f. Such a small increase is at the detection level of the data set used in this study. This estimate of freeboard change is based on the hydrostatic balance equation $\Delta h_f = \Delta h \frac{\rho_w - \rho_i}{\rho_w}$, where $\rho_w = 1,025$ kg/m^3 is sea water density and $\rho_i = 906$ kg/m^3 is sea ice density measured for first year ice at R/V *Lance* (Gerland et al., 2017). Hereafter, all the sea ice thickness change values in this paper were calculated by this formula.

We used the distance x, y between the virtual buoys and the distance covered by them in the time between the overflights (velocities u, v) to calculate the partial derivatives $\frac{\partial u}{\partial x}$, $\frac{\partial u}{\partial y}$, $\frac{\partial v}{\partial x}$, and $\frac{\partial v}{\partial y}$. This gives us the divergence

$$\epsilon_{\text{div}} = \frac{\partial u}{\partial x} + \frac{\partial v}{\partial y}, \tag{1}$$

and the maximal shear rate

$$\epsilon_{\text{shr}} = \sqrt{\left(\frac{\partial u}{\partial x} - \frac{\partial v}{\partial y}\right)^2 + \left(\frac{\partial u}{\partial y} + \frac{\partial v}{\partial x}\right)^2} \tag{2}$$

of each individual triangle. Since the resolution of the freeboard maps is 5 m × 5 m, we estimated that a virtual buoy could be placed erroneously by 1 grid point or 5 m. This makes the accuracy of the relative positions of the virtual buoys $\delta_x \approx 5$ m. According to Hutchings et al. (2012) the error of the deformation estimate becomes negligible when $A >> 8N^2\delta_x^2 = 1,800$ m^2, where $N = 3$ is the number of buoys. This holds for all triangles as they are much larger than 1,800 m^2. The triangles were carefully placed in a way to minimize loss of the sea ice mass through the triangle boundaries. This partly mitigates the data sampling problem for sea ice deformation described in Bouillon and Rampal (2015), and we therefore did not apply further filtering.

Additionally, the deformation was calculated by the same procedure for a GPS drifter array (Itkin et al., 2017) that was deployed before and between the overflights (Figures 1a and 1b). Note that the deformation rate magnitudes are scale dependent (Hutchings et al., 2012; Itkin et al., 2017). During the first overflight the array was composed of three drifters covering a triangle with sides up to 100 km south of R/V *Lance* position. The number of drifters in the array gradually increased by further deployments in the following days, and from 21 April deformation could be calculated on a length scale of 10–15 km (Figure 1b). During the second overflight there were altogether 11 drifters deployed in the larger vicinity of the freeboard data presented here.

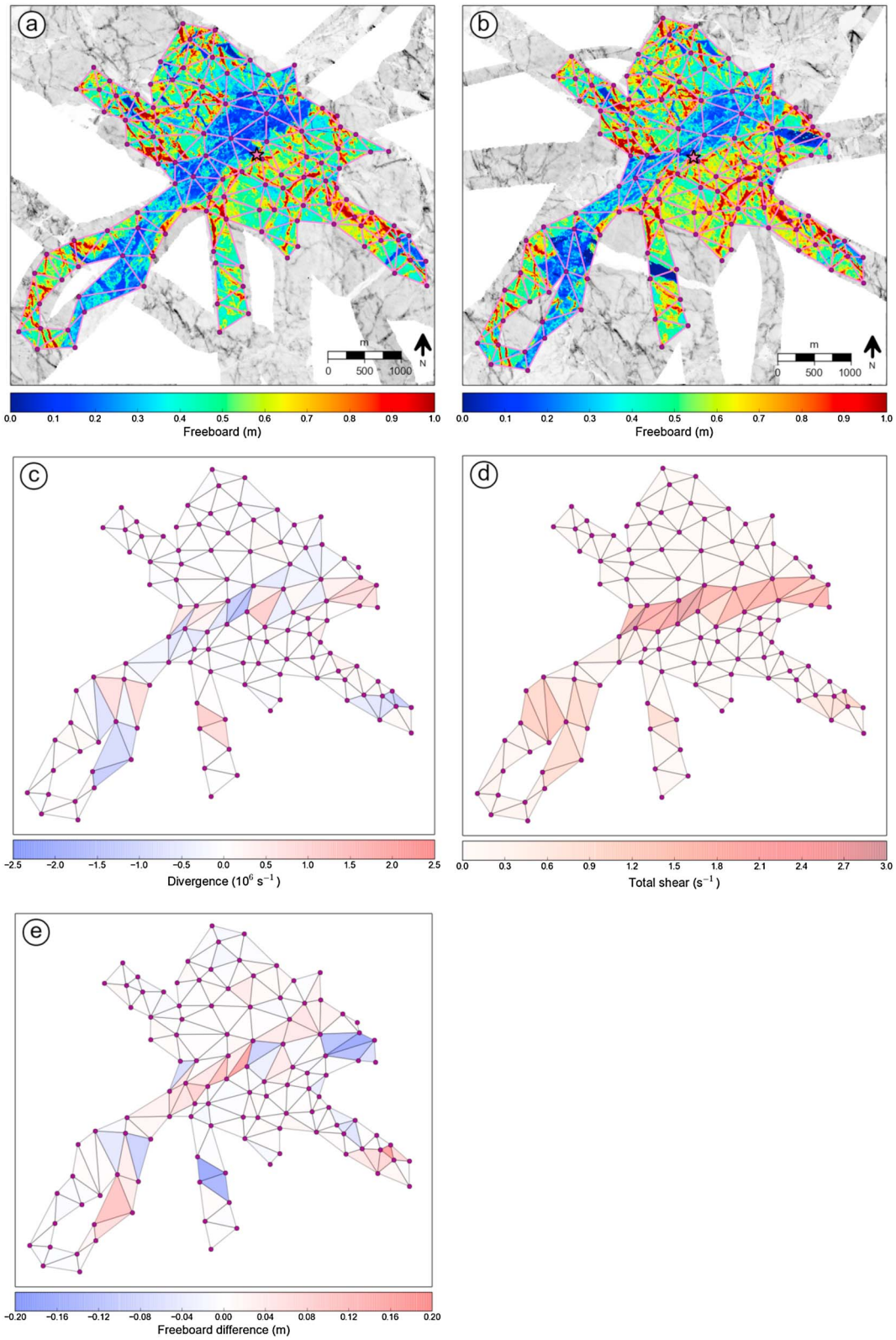

Figure 2. (a and b) Freeboard maps for the overflights on 19 and 24 April. The virtual buoys are marked with purple dots. Lines depict the triangles between them. Position of R/V *Lance* is marked by pink star in the centers of the maps. Freeboards of the survey region are depicted in colors as shown by the colorbar. The measured freeboards out of that region are depicted in gray shading where light/dark areas represent low/high values. (c) Divergence. (d) Total shear. (e) Freeboard change measured for the triangles between the overflights.

The map in Figure 1a shows the position of nine drifters during second overflight, the rest are outside the map. The time series of deformation from these drifters (Figure 1b) show the convergent motion during and right after the first overflight, followed by a divergent motion during which open water was observed around R/V *Lance*. Prior to the second overflight the pack closed in on *Lance* by strong convergence coinciding with strong northerly winds (Hudson et al., 2015).

To quantify the role of deformation for the freeboard changes, we adopted a linear regression model for divergence ϵ_{div}: $\Delta h_f = \alpha\epsilon_{\text{div}} + \beta$, where α is the slope of the regression line and β is the intercept that represents residuals originating, for example, from shear ϵ_{shr} and thermodynamical sea ice growth Δh_t. For shear and combined divergence and shear an accordant regression can be formulated.

3. Results and Discussion

During the first overflight there were two active leads in the vicinity of R/V *Lance* (Figure 2a). They were running in parallel in the SW-NE direction spaced by about 2 km. The larger of them stretched in the center of the matched overflight area and was about 2 km wide. It was composed of two different regimes: a 0.5 to 1 km wide belt of uniform young ice on the SE side (adjacent to R/V *Lance*) and a belt of fragmented ice floes with diameter ~500 m with thin ice in the narrow cracks between them. The smaller lead on the SE edge of the area was ~100 m wide. None of the leads had open water.

Between the overflights there was a strong shearing motion along a crack running roughly in E-W direction in the wide lead, where the opposite sides of the lead moved some 200 m relatively to each other (Figure 2b). This deformation caused the thin ice in the wide lead to compress and raft (Figure 3a). Some new ridges were also formed. Along the same shear line in the eastern part of the surveyed region a new lead opened (Figure 3c). The smaller lead on the SE edge of the area closed completely, and a new ridge was formed along the edges there (Figure 3b). Additionally, there was a large new lead with large areas of open water in the southern part of the survey region.

The divergence calculated for the triangles between the virtual buoys was first used to sort the triangles into three classes: those that did not deform significantly ($|\epsilon_{\text{div}}| < 0.110^6$), those that diverged, and those that converged. Plots of PDFs of freeboard were made for each class (Figures 3d–3f). While all three PDFs are bimodal, the low freeboard mode is much more expressed for the classes that deformed. This points toward the fact that mainly thin sea ice deformed. In the PDF for the divergent triangles (Figure 3f) the low freeboard mode and open water fraction increased before the second overflight, which is a consequence of thin ice and open water in the leads. The divergent area increased by 55%, which is 4% of the survey region. The PDF for the converging triangles (Figure 3e) shows a reduction in the low freeboard mode and an increase of freeboards between the modes, in the high freeboard mode and in the tail of the distribution. This indicates an increase in freeboard by rafting and ridging. The convergent area decreased by 23%, which is 4% of the survey region. The mean freeboard values of both overflights $\bar{h}_f$ and average divergence $\bar{\epsilon}_{\text{div}}$ are written in Figures 3d, 3f, and 3g. The criteria of mass conservation were used in applying postprocessing corrections (for details, see supporting information). After the corrections the PDF for nondeformed triangles (Figure 3d) offers a visual check that the sea ice mass was conserved between the overflights.

Based on Figure 3e, we determined 0.25±0.05 m as a threshold freeboard value between thin and thick ice. This is the value below that the ice freeboard probability decreased in the time between the overflights. Then we constructed a PDF for the whole survey region (a sum of all PDFs in Figures 3d–3f, shown also in Figure S3 in the supporting information). The thick ice freeboard values increased by 1.3±0.3%, and the same amount of sea ice volume was redistributed from level thin ice into deformed ice.

The contribution of the deformation to the sea ice mass redistribution was quantified by a linear regression between the deformation (divergence and shear) and freeboard change (Figure 4). The linear model with divergence shows a clear statistical relationship between divergence and freeboard change, and it explains 64% of freeboard change variability (Figure 4a). There is no statistical relationship between shear and freeboard change as shear alone (without convergence) should not contribute to any mass redistribution. In combination with convergence, shear often causes stronger rafting and ridging, so for convergent triangles shear rate can explain 32% of freeboard change variability (Figure 4b). Although this means that divergence and shear are not independent variables, Kwok and Cunningham (2016) combined the effect of both strain

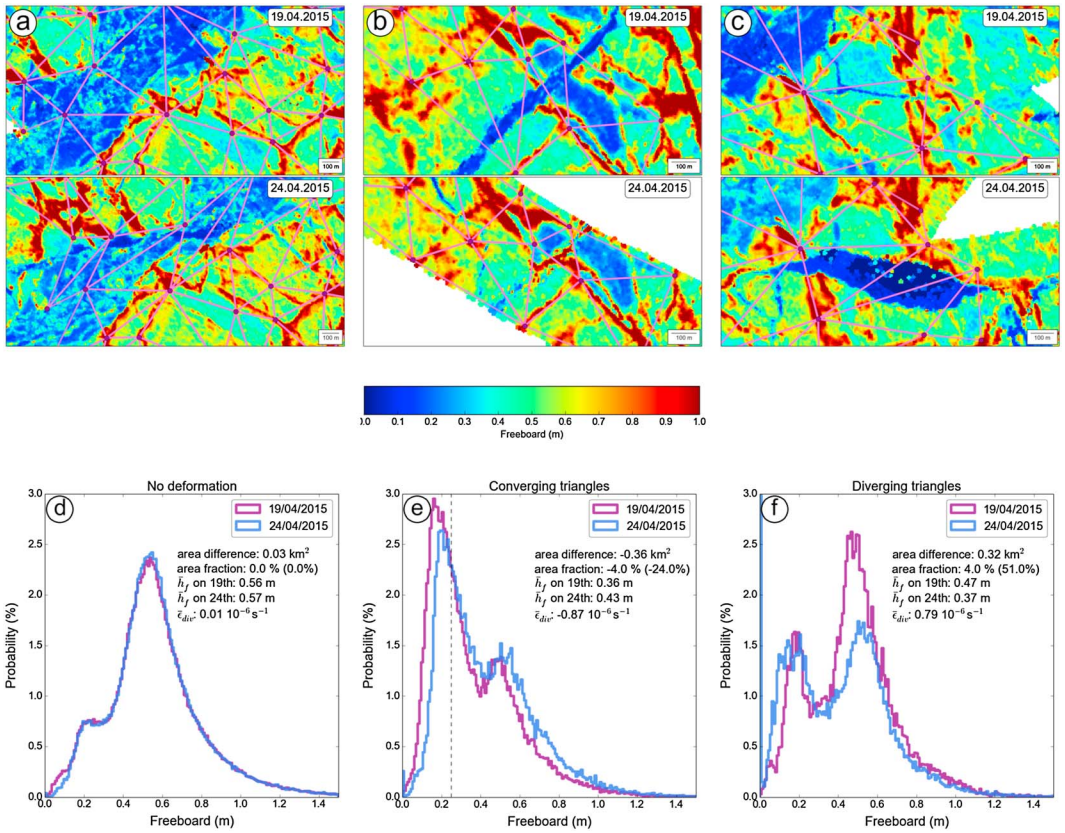

Figure 3. Examples of sea ice deformation and ice mass redistribution with enlargements from Figures 2a and 2b: (a) rafting (central part of the large lead), (b) ridging (small lead and ridged area in the center right), and (c) new lead (in the upper right corner). PDFs of freeboard for the triangles with (d) no deformation, (e) convergence, and (f) divergence. The text on the individual panels shows absolute and relative changes in area of triangles (in brackets fraction of total survey region area), mean freeboard $\bar{h}_f$ for both overflights, and mean divergence rate $\bar{\epsilon}_{\mathrm{div}}$. Dash vertical line in Figure 3e shows the threshold value between the thin and thick ice.

rates in a multiple regression model $\Delta h = \alpha\epsilon_{\mathrm{div}} + \beta\epsilon_{\mathrm{shr}} + \Delta h_t$. Following their method adjusted squared correlation amounts to 65%, which means that shear cannot explain much additional variability and that divergence is a good single predictor of sea ice mass redistribution in our case.

The slope α for the linear model in Figure 4a is −0.1, signifying that at the 100–500 m scale of the triangles an increase in convergence of 1×10^6 will cause an increase in freeboard of 0.1 m. The slope $\alpha = 0.036$ for the linear model in Figure 4b shows a more moderate gain of mass for a similar increase in shear in the convergent cases. The residuals Δh_t as well as β of the models in Figures 4a and 4b are small (0.003, 0.001, and 0.011) and satisfy our assumption about negligible thermodynamical growth and snow accumulation in the 5 days between the overflights.

Our results suggest that convergence, in this case, is limited to initially thin ice. This is clearly visible in Figure 4a, where the strongest convergence occurs only in triangles that initially had the lowest freeboards (blue dots). Divergence can, on contrary, occur also at higher freeboards. Oikkonen et al. (2017) showed that new leads often occur along existent lines of damage, for example, cracks formed by shear. Development of a lead from such a crack is visible in Figure 3c.

The strong statistical relationship between divergence and freeboard change indicates that this rule can be applied in a more general way, despite the fact that deformation depends on external forcing and internal sea ice strength, where relationships are nonlinear. For the regions similar to ours, in the Transpolar Drift, that are not confined by land masses and where shear does not play such an important role as, for example, in the sea ice covered region north of Greenland and Canadian Archipelago, and if temporal and spatial scaling of sea ice deformation are considered, our statistical model offers an opportunity for numerical model validations.

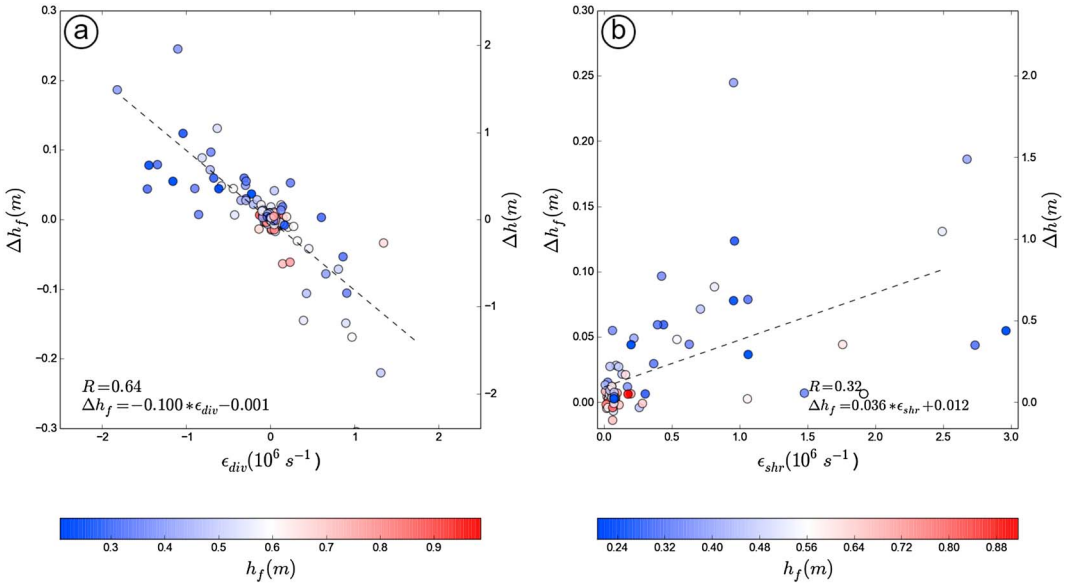

Figure 4. Relationships between deformation and freeboard changes Δh_f: (a) divergence ϵ_{div} and (b) shear ϵ_{shr} only for the convergence cases. The panels depict the squared correlation R and the regression models, where the coefficients are α and β. Both regressions are statistically significant at 99% confidence levels. The color of the markers gives initial freeboard.

4. Conclusions

This case study analyzes a set of unique repeated airborne measurements of sea ice freeboard in April 2015 north of Svalbard. Sea ice mass balance change was estimated based on freeboard heights derived from laser scanner data, and deformation was calculated from the displacement of virtual buoys identified in the data before and after a storm event. Our results show that most of the deformation and freeboard changes were confined to the initially thin ice areas originating from previous lead-forming deformation events. Our linear regression model shows that typical divergence value of $\pm 2 \times 10^{-6}$ s^{-1} will lead to $\pm$0.2 m change in freeboard. Taking into account the in situ sea ice density measurements in the survey region (Gerland et al., 2017) that yields in about 1.5 m change in sea ice thickness.

The thin ice areas were reduced by 4% and transformed into deformed ice as a consequence of this storm. At the same time 4% of area was covered with new leads where ice grew thermodynamically until melt onset in summer and therefore contributed to an increase in ice volume. This suggests that even if the total sea ice area remains constant like in our case, the sea ice volume is continuously growing. For example, at a mean temperature of −20°C, there would be a 0.22 m thick layer of thin ice thermodynamically formed in the open water leads after 1 week according to the empirical formula of Lebedev (Maykut, 1986). The in situ measured mean sea ice thickness from various types of ice in the vicinity of the research ship was 1.45 m (A. Rösel, personal communication, 2017). Assuming that this is representative also for mean sea ice thickness in the rest of the survey region with a total size of 9.05 km^2, the new thin ice covering the area of 0.32 km^2 (area increase of diverging triangles in Figure 3f), would add 0.5% of sea ice volume.

The sea ice north of Svalbard is impacted by 10 to 20 storms every winter (Rinke et al., 2017). Assuming that other storms have a similar effect on the ice volume, this would result in 5 to 10% volume increase caused by deformation based on the 0.5% volume increase observed for the analyzed storm. Likewise, in the deformation event associated with the storm about 1.3% of survey region ice volume was deformed to rafted ice and ridges, which would by similar multiplication with the number of storms result in about 13 to 26% fraction of deformed ice at the end of the winter. Such simplified extrapolation provides an estimate that is of same order of magnitude as the 30% deformed ice fraction measured by long time series provided by moored upward looking sonars downstream in Fram Strait (Hansen et al., 2013). Finally, sea ice thickness measurements on snow-covered level ice showed that there was no significant thermodynamical growth outside the refrozen leads in the region from January to June (Itkin et al., 2015), which makes the dynamic processes a major driver of the sea ice volume gain in this period.

Acknowledgments
We deeply thank the crew and scientists on board BAS Twin Otter airplane and R/V *Lance* for their hard work during the airplane overflights. The field campaign and associated data and processing and analysis have been funded by the EU ICE-ARC project (paper ICE-ARC-020) and the Norwegian Polar Institute's Centre for Ice, Climate and Ecosystems (ICE) through the N-ICE project. P. I. was also supported by ID Arctic (funded the by Norwegian Ministries of Foreign Affairs and Climate and Environment, programme Arktis 2030). G. S. was supported by the Transregional Collaborative Research Center (TR 172). "ArctiC Amplification: Climate Relevant Atmospheric and SurfaCe Processes, and Feedback mechanisms (AC)3" funded by the German Research Foundation (DFG, Deutsche Forschungsgemeinschaft). All in situ data used in this paper are published in the Norwegian Polar Institute database http://data.npolar.no. The airborne data from the campaign are available from the ICE-ARC project repository http://ice2seadata.nerc-bas.ac.uk/.

References

Bouillon, S., & Rampal, P. (2015). On producing sea ice deformation data sets from SAR-derived sea ice motion. *The Cryosphere*, *9*(2), 663–673. https://doi.org/10.5194/tc-9-663-2015

Cohen, L., Hudson, S. R., Walden, V. P., Graham, R. M., & Granskog, M. A. (2017). Meteorological conditions in a thinner Arctic sea ice regime from winter through summer during the Norwegian Young Sea Ice expedition (N-ICE2015). *Journal of Geophysical Research: Atmospheres*, *122*, 7235–7259. https://doi.org/10.1002/2016JD026034

Gerland, S., Granskog, M. A., King, J., Rösel, A., & Itkin, P. (2017). *N-ICE2015 ice core physics: Temperature, salinity and density*. Norway: Norwegian Polar Institute. https://doi.org/10.21334/npolar.2017.c3db82e3

Granskog, M. A., Assmy, P., Gerland, S., Spreen, G., Steen, H., & Smedsrud, L. H. (2016). Arctic research on thin ice: Consequences of Arctic sea ice loss. *Eos Transactions American Geophysical Union*, *97*, 22–26. https://doi.org/10.1029/2016EO044097

Hansen, E., Gerland, S., Granskog, M. A., Pavlova, O., Renner, A. H. H., Haapala, J., … Tschudi, M. (2013). Thinning of Arctic sea ice observed in Fram Strait: 1990–2011. *Journal of Geophysical Research: Oceans*, *118*, 5202–5221. https://doi.org/10.1002/jgrc.20393

Hudson, S. R., Cohen, L., & Walden, V. (2015). *N-ICE2015 surface meteorology*. Norwegian Polar Institute. https://doi.org/10.21334/npolar.2015.056a61d1

Hutchings, J. K., Roberts, A., Geiger, C. A., & Richter-Menge, J. (2011). Spatial and temporal characterization of sea-ice deformation. *Annals of Glaciology*, *52*(57), 360–368.

Hutchings, J. K., Heil, P., Steer, A., & Hibler, W. D. (2012). Subsynoptic scale spatial variability of sea ice deformation in the western Weddell Sea during early summer. *Journal of Geophysical Research*, *117*, C01002. https://doi.org/10.1029/2011JC006961

Hvidegaard, S. M., & Forsberg, R. (2002). Sea-ice thickness from airborne laser altimetry over the Arctic Ocean north of Greenland. *Geophysical Research Letters*, *20*(29), 1952. https://doi.org/10.1029/2001GL014474

Itkin, P., Spreen, G., Cheng, B., Doble, M., Gerland, S., Granskog, M. A., … Helgeland, C. (2015). *N-ICE2015 buoy data*. Norwegian Polar Institute. https://doi.org/10.21334/npolar.2015.6ed9a8ca

Itkin, P., Spreen, G., Cheng, B., Doble, M., Girard-Ardhuin, F., Haapala, J., … Wilkinson, J. (2017). Thin ice and storms: Sea ice deformation from buoy arrays deployed during N-ICE2015. *Journal of Geophysical Research: Oceans*, *122*, 4661–4674. https://doi.org/10.1002/2016JC012403

Kwok, R., & Cunningham, G. (2015). Variability of Arctic sea ice thickness and volume from CryoSat-2. *Philosophical Transactions of the Royal Society A: Mathematical, Physical and Engineering Sciences*, *373*, 20140157. https://doi.org/10.1098/rsta.2014.0157

Kwok, R., & Cunningham, G. F. (2016). Contributions of growth and deformation to monthly variability in sea ice thickness north of the coasts of Greenland and the Canadian Arctic Archipelago. *Geophysical Research Letters*, *43*, 8097–8105. https://doi.org/10.1002/2016GL069333

Maykut, G. A. (1986). *The surface heat and mass balance* (pp. 395–463). Boston, MA: Springer. https://doi.org/10.1007/978-1-4899-5352-0_6

Oikkonen, A., Haapala, J., Lensu, M., Karvonen, J., & Itkin, P. (2017). Small-scale sea ice deformation during N-ICE2015: From compact pack ice to marginal ice zone. *Journal of Geophysical Research: Oceans*, *122*, 5105–5120. https://doi.org/10.1002/2016JC012387

Rampal, P., Weiss, J., & Marsan, D. (2009). Positive trend in the mean speed and deformation rate of Arctic sea ice, 1979–2007. *Journal of Geophysical Research*, *114*, C05013. https://doi.org/10.1029/2008JC005066

Rinke, A., Maturilli, M., Graham, R., Matthes, H., Handorf, D., Cohen, L., … Moore, J. C. (2017). Extreme cyclone events in the Arctic: Wintertime variability and trends. *Environmental Research Letters*, *12*(9), 094006. https://doi.org/10.1088/1748-9326/aa7def

Rösel, A., Polashenski, C. M., Liston, G. E., King, J. A., Nicolaus, M., Gallet, J.-C., … Granskog, M. A. (2016). *N-ICE2015 snow depth data with magna probe*. Norwegian Polar Institute. https://doi.org/10.21334/npolar.2016.3d72756d

Spreen, G., Kwok, R., & Menemenlis, D. (2011). Trends in Arctic sea ice drift and role of wind forcing: 1992–2009. *Geophysical Research Letters*, *38*, L19501. https://doi.org/10.1029/2011GL048970

Thorndike, A. S. (1986). *Kinematics of sea ice* (pp. 489–549). Boston, MA: Springer. https://doi.org/10.1007/978-1-4899-5352-0_8